

# LINEAR BEAM–BEAM RESONANCES DUE TO COHERENT DIPOLE MOTION

KOJI HIRATA<sup>1</sup> and EBERHARD KEIL<sup>2</sup>

<sup>1</sup>KEK, National Laboratory for High Energy Physics, Tsukuba, 305, Japan  
<sup>2</sup>CERN, Geneva, Switzerland

(Received 24 January 1996; in final form 8 May 1996)

We study the transverse motion of the barycentres of bunches in two beams that circulate in opposite direction in a storage ring, and are coupled by the beam–beam effect. The motion is described by a linear system of oscillators, and represented by a matrix. We distinguish between perfect machines in which the bunch parameters and the arc and interaction point parameters are all equal, and machines with errors in which at least one of these conditions is not satisfied. We determine the regions in tune space where the motion is unstable, analytically for perfect machines, and numerically for machines with errors. We identify these regions as resonances related to the tunes of one of the two beams or to their sum. We establish which resonances are excited under given conditions. We find that more resonances occur in machines with errors than in perfect machines. By multi-particle tracking, we study the instability at finite amplitudes.

*Keywords:* Colliding beams; instabilities; resonances; storage rings.

## 1 INTRODUCTION

The beam–beam interaction is one of the major performance limitations of circular colliders and has been studied theoretically, experimentally and by computer simulation for a long time. Several effects of this interaction can be studied by assuming that the bunches behave as rigid bodies: in the Rigid Gaussian Model (RGM)<sup>1,2</sup>, we assume that the density distributions are a Gaussian with fixed beam radii, and apply the beam–beam forces between the barycentres.

Carrying the simplification one step further, and limiting ourselves to the study of the small amplitude oscillation of the bunches around the closed orbit, we can linearize the beam–beam force and reduce the study of the bunch motion to the study of the symplectic one-turn matrix. This Linear RGM (LRGM)<sup>3</sup> addresses the following main issues:

*Beam–Beam Modes:* When the motion of the bunches is stable, the eigenvalues of the one-turn matrix yield the visible betatron tunes, i.e. betatron frequencies divided by the revolution frequency, each corresponding to a coherent dipole oscillation mode of the system of oscillating bunches. They are used in setting up colliders such that the luminosity reaches a maximum.<sup>4–7</sup>

*Linear Beam–Beam Resonances:* Whenever an eigenvalue exceeds unity in absolute value, the motion becomes unstable. The LRGM yields the conditions when the instability takes place. It explained why space charge compensation with four beams in the ‘Dispositif à Collisions dans le Igloo’ (DCI)<sup>8</sup> did not work as originally planned.<sup>9,10</sup> The LRGM also gave the argument for abandoning the idea of building high-luminosity B (and other) factories composed of two rings with different circumferences.<sup>1,11</sup>

Piwinski<sup>12</sup> was the first to use the eigenvalue technique. He treated a whole bunch as a point particle, found an instability when integral and half-integral tunes are approached from below (above) for attractive (repulsive) beam–beam forces, and gave a closed expression for the threshold of the instability. Our work can be thought of as a refinement and a generalization of Piwinski’s approach.

Chao and Keil<sup>13</sup> demonstrated that half-integral resonances are not excited in the case of  $N$  bunches in each beam colliding at  $2N$  interaction points (IPs) in a symmetric machine, and also found more resonances in machines with phase errors between the interaction points. They identified these resonances as complex resonances: a pair of complex eigenvalues become larger than unity in absolute value. Keil continued the linear analysis and found that resonances growing out of the half-integral tunes are a generic feature of machines with phase advance errors between the collision points.<sup>14</sup> He computed the visible tunes, and demonstrated that resonances arise when two visible tunes meet.<sup>15</sup> In the study of coherent beam–beam effects in the SSC, Chao and Furman<sup>16,17</sup> found half-integral resonances, which they called sail-shaped objects.

Keil used a multi-particle tracking code<sup>18</sup> to compute the relation between the beam–beam strength parameter  $\xi$  and the visible frequencies of the barycentre modes ( $\sigma$  and  $\pi$ ). He found that the frequency difference was about a factor of two smaller than expected from Piwinski’s theory.<sup>12</sup> Hirata<sup>3</sup> showed that in the RGM the slope of the force between two bunches is a factor of two smaller than that between a bunch and a test particle, when the

collisions are head-on. Hofmann and Myers<sup>19</sup> obtained the same result. It was confirmed experimentally in the SLC.<sup>20</sup> Our LRGM includes this effect.

Based on the LRGM, we constructed a computer code, BBMODE<sup>21</sup>, which finds the eigenvalues and allows all possible errors. When we apply BBMODE to LEP with various errors, we find many narrow resonances in surprisingly complicated patterns.<sup>22</sup> A systematic survey of all these resonances is one of the purposes of the present paper.

We assume throughout that the  $N$  equidistant bunches of the  $e^+$  beam and the  $N$  equidistant bunches of the  $e^-$  beam circulate in opposite directions in a single storage ring or in two rings of the same circumference. In a single ring,  $2N$  equidistant interaction points are possible at most. When all of them except  $N_{\text{IP}}$  are made inactive by separating the two beams, we denote this case as  $N \oplus N = N_{\text{IP}}$ . We distinguish between perfect machines in which the bunch parameters and the arc and interaction point parameters are all equal, and machines with errors in which at least one of these conditions is not satisfied. Whenever we can relax this most restrictive definition of a perfect machine, we shall explicitly state it. However, the phase advances of the two beams in the arcs need not be the same. When we calculate growth rates of the beam-beam modes, we do not include any damping mechanism, e.g. synchrotron radiation damping, feedback systems, and Landau damping.<sup>6</sup>

Our paper is organized as follows. In Section 2, we summarize the Linear Rigid Gaussian Model and its simplest application to the  $1 \oplus 1 = 1$  case. In Section 3, we study perfect machines. Section 4 is devoted to machines with errors. Section 5 contains the discussion of the complex resonances, and Section 6 our conclusions. Appendix A contains mathematical lemmas which allow the reduction of the  $N \oplus N = N_{\text{IP}}$  case to the  $N' \oplus N' = N_{\text{IP}}$  case, where  $N' \leq N$ . Appendix B compares the results of the LRGM and multi-particle tracking.

## 2 MACHINES WITH ONE INTERACTION POINT

Here, we introduce the notation, and describe the simplest case ( $1 \oplus 1 = 1$ ) in detail, including all possible differences between bunches and the arcs. We denote the tune of the  $e^\pm$  beam without the beam-beam effect as  $Q_z^\pm$  ( $z$  stands for either  $x$ , horizontal, or  $y$ , vertical). The revolution matrix for the  $z$  coordinate is given by

$$M_z = \hat{U}(Q_z^+, Q_z^-)R(\Xi_z^+, \Xi_z^-). \quad (1)$$

The transformations  $\hat{U}$  through the arcs are block-diagonal  $4 \times 4$  matrices:

$$\hat{U}(Q^+, Q^-) = \begin{pmatrix} U(Q^+) & O \\ O & U(Q^-) \end{pmatrix}, \quad (2)$$

$$U(Q) = \begin{pmatrix} \cos 2\pi Q & \sin 2\pi Q \\ -\sin 2\pi Q & \cos 2\pi Q \end{pmatrix}.$$

Here  $O$  is the null matrix of suitable dimension whose components are 0. The revolution matrix  $M_z$  operates on the dynamical variables

$$\begin{pmatrix} \mathbf{Z}_+ \\ \mathbf{Z}_- \end{pmatrix} \quad \text{where} \quad \mathbf{Z}_\pm = \sqrt{N_\pm} \gamma_\pm \begin{pmatrix} z_\pm \\ \alpha_z^\pm z_\pm / \sqrt{\beta_z^\pm} + \sqrt{\beta_z^\pm} z'_\pm \end{pmatrix}. \quad (3)$$

Here,  $N_\pm$  is the number of particles,  $\gamma_\pm$  is the relativistic Lorentz factor,  $z_\pm$  is the  $z$  coordinate of the barycentre,  $z'_\pm$  is its slope, and  $\alpha_z^\pm$  and  $\beta_z^\pm$  are nominal Twiss parameters of the  $e^\pm$  beam at the IP. The beam-beam kick matrix  $R$  is defined by:

$$R(\Xi_z^+, \Xi_z^-) = \begin{pmatrix} I - A(\Xi_z^+) & A(\sqrt{\Xi_z^+ \Xi_z^-}) \\ A(\sqrt{\Xi_z^+ \Xi_z^-}) & I - A(\Xi_z^-) \end{pmatrix}, \quad A(\Xi) = \begin{pmatrix} 0 & 0 \\ 4\pi \Xi & 0 \end{pmatrix}, \quad (4)$$

with the coherent beam-beam parameter,  $\Xi_z^\pm$ ,

$$\Xi_z^\pm = \frac{r_e N_\mp \beta_z^\pm Y_z}{2\pi \gamma_\pm \Sigma_z (\Sigma_x + \Sigma_y)}, \quad \Sigma_z = \sqrt{(\sigma_z^+)^2 + (\sigma_z^-)^2}. \quad (5)$$

Here and in the following,  $I$  is the unit matrix of suitable dimension,  $r_e$  is the classical electron radius, and  $Y_z$  is the Yokoya factor. This factor describes the change of the visible tunes caused by the distortion of the beam distribution by the beam-beam collision.<sup>a</sup> We have assumed that the force is attractive.

<sup>a</sup>It should be noted that (5) is only phenomenologically correct for head-on collision. Meller and Siemann<sup>23</sup> and Yokoya and Koiso<sup>24</sup> calculated the beam-beam effect on the coherent tunes for head-on beam-beam collisions and found that the visible tune difference is larger than what we expect from the LRGM. We include this effect by multiplying the focusing force with a phenomenological factor which we call Yokoya factor  $Y_z$ . Typical values for flat beams with  $\sigma_y \ll \sigma_x$  are  $Y_x \approx 1.33$  and  $Y_y \approx 1.24$ . The factor is not known for cases with an offset between the axes of the two beams of the order of the beam sizes or larger, and this simple treatment is no longer accurate. Beam-beam collisions with an offset also change the closed orbits of the bunches.<sup>2</sup> To treat such cases, we should go beyond the linear analysis. In most of this paper, we shall confine ourselves to the case where the collision is head-on.

For a repulsive force, the sign of  $\Xi$  should be changed. When  $\sigma^+ = \sigma^-$ , we have  $\Xi_z = Y_z \xi_z / 2$ , where  $\xi_z$  is the usual beam-beam parameter

$$\xi_z^\pm = \frac{r_e N_{\mp} \beta_z^\pm}{2\pi \gamma_{\pm} \sigma_z^{\mp} (\sigma_x^{\mp} + \sigma_y^{\mp})}. \quad (6)$$

As is clear from (4), the beam-beam collision is represented by  $\Xi_z^\pm$  only: any difference in  $N^\pm$ ,  $\beta_z^\pm$ ,  $\alpha_z^\pm$ ,  $\gamma^\pm$ ,  $\sigma_x^\pm$ , and  $\sigma_y^\pm$  is taken into account. As long as the collision is head-on and the directions of the betatron modes are the same in the  $e^+$  and  $e^-$  beams, the linear motions in the  $x$  and  $y$  degrees of freedom are independent. We assume this to be the case and drop the subscripts  $z$  hereafter.

Since  $M$  is a symplectic  $4 \times 4$  matrix, we can use a well-known technique<sup>25</sup> to obtain the average of the eigenvalue  $\lambda$  and its reciprocal  $1/\lambda$ :

$$\begin{aligned} \cos \bar{\mu}^\pm &= \frac{\lambda + 1/\lambda}{2} = \frac{\cos \mu^+ + \cos \mu^-}{2} \\ &\quad - \pi \Xi^+ \sin \mu^+ - \pi \Xi^- \sin \mu^- \pm \frac{1}{2} \sqrt{D}, \end{aligned} \quad (7)$$

$$\begin{aligned} D &= [\cos \mu^+ - \cos \mu^- - 2\pi \Xi^+ \sin \mu^+ + 2\pi \Xi^- \sin \mu^-]^2 \\ &\quad + 16\pi^2 \Xi^- \Xi^+ \sin \mu^+ \sin \mu^-. \end{aligned} \quad (8)$$

The mapping  $M$  is stable if and only if both  $\cos \bar{\mu}^+$  and  $\cos \bar{\mu}^-$  are real and fall into the region between  $-1$  and  $+1$ . The mapping is unstable, in terms of  $Q^\pm$  and  $D$ , if:

- $D > 0$  and  $Q^+ \lesssim$  integer or  $Q^- \lesssim$  integer, then one  $\lambda$  is real and  $\lambda > 1$ . We call this a positive or integral resonance.
- $D > 0$  and  $Q^+ \lesssim$  half-integer or  $Q^- \lesssim$  half-integer, then one  $\lambda$  is real and  $\lambda < -1$ . We call this a negative or half-integral resonance.
- $D < 0$  and  $Q^+ + Q^- \lesssim$  integer, then there is a complex conjugate pair of  $\lambda$ 's with  $|\lambda| > 1$ . We call this a complex or sum resonance.

Here,  $Q^+ \lesssim$  integer, for example, indicates that the instability occurs when  $Q^+$  approaches the integer from below. The instability does not necessarily persist until  $Q^+$  reaches the integer. More than one type of resonance can occur at the same tunes.

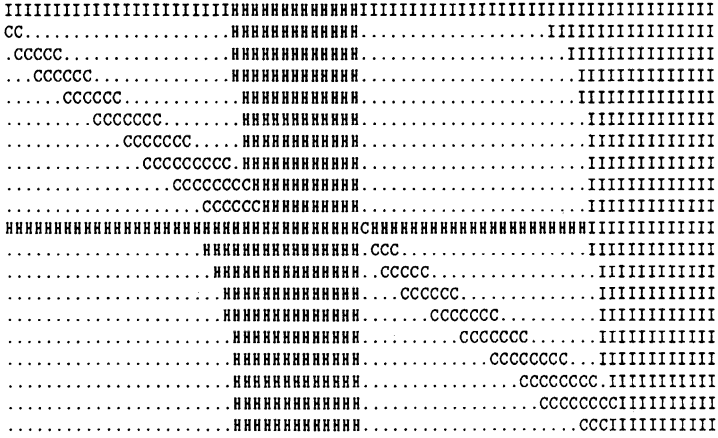


FIGURE 1 Unstable region in tune space for the  $1 \oplus 1=1$  case with  $\Xi^+ = 0.1$  and  $\Xi^- = 0.01$ . The abscissa is  $0 \leq Q^+ \leq 1$ , the ordinate is  $0 \leq Q^- \leq 1$ . The type of eigenvalue with the largest growth rate is indicated: H, I and C stand for half-integral, integral and complex sum resonances, respectively. The pattern repeats itself with period 1 for  $Q^+$  and  $Q^-$ .

The unstable region in the  $(Q^+, Q^-)$ -plane is shown in Figure 1, which displays a case with  $\Xi^+ \neq \Xi^-$ . All unstable regions listed above can be seen clearly. As is clear from (1), under a replacement  $(Q^+, Q^-) \rightarrow (Q^+ + 1/2, Q^- \pm 1/2)$ ,  $M$  becomes  $-M$ , so that  $\lambda$  remains the same but with opposite sign. This is the reason why, in Figure 1,  $(0 \leq Q^+ \leq 1/2, 0 \leq Q^- \leq 1/2)$  and  $(1/2 \leq Q^+ \leq 1, 1/2 \leq Q^- \leq 1)$  and also  $(0 \leq Q^+ \leq 1/2, 1/2 \leq Q^- \leq 1)$  and  $(1/2 \leq Q^+ \leq 1, 0 \leq Q^- \leq 1/2)$  are identical apart from the replacement  $H \leftrightarrow I$ , forming a chessboard pattern. For  $\Xi^+ = \Xi^-$ , the graph would be symmetric under the reflection with respect to the line  $Q^+ = Q^-$ .

### 3 PERFECT MACHINES

Here, we consider cases of machines with equally spaced bunches and equally spaced IPs. All bunches and IPs are equal, i.e.  $\Xi^+ = \Xi^- = \Xi$ . The phase advances  $2\pi\nu_+$  for the  $e^+$  beam in the arcs connecting the IPs are all the same, and so are the phase advances  $2\pi\nu_-$  of the  $e^-$  beam. However,  $\nu_+$  and  $\nu_-$  may be different. The eigenvalues can be found analytically.

In some cases, the problem is reducible: The  $2 \oplus 2 = 2$  case splits into two mutually independent and identical  $1 \oplus 1 = 2$  cases with the same eigenvalues. We have to examine only the irreducible cases. The number of such cases is not large. We prove in Appendix A that  $N \oplus N = N$  (with odd  $N$ ) and  $N \oplus N = 2N$  are the only irreducible cases with equally spaced IPs. We begin with the  $3 \oplus 3 = 3$  and  $3 \oplus 3 = 6$  cases, because  $N = 3$  is the smallest  $N$  which contains all essential features of cases with  $N \geq 3$ . We then treat the  $N \oplus N = N$  and  $N \oplus N = 2N$  cases. Finally, we derive a closed expression for the threshold of the instability for the general  $N \oplus N = N_{\text{IP}}$  case.

### 3.1 The $3 \oplus 3 = 3$ Case

We use the Eulerian view<sup>26</sup>; instead of labelling the bunches and following them around the ring, we label the IPs, and call them  $\text{IP}_1$ ,  $\text{IP}_2$ , and  $\text{IP}_3$  in a clockwise manner, and we give the bunches, which collide there at a particular instant in time, the label of the IP. We define the state vector  $\mathbf{Y} = (\mathbf{Y}_1, \mathbf{Y}_2, \dots, \mathbf{Y}_6)^t$ , where,

$$\begin{array}{ll} \mathbf{Y}_1 : e^+ \text{ at IP}_1 & \mathbf{Y}_4 : e^- \text{ at IP}_1 \\ \mathbf{Y}_2 : e^+ \text{ at IP}_2 & \mathbf{Y}_5 : e^- \text{ at IP}_2 \\ \mathbf{Y}_3 : e^+ \text{ at IP}_3 & \mathbf{Y}_6 : e^- \text{ at IP}_3 . \end{array}$$

Let  $\mathbf{Y}_1$  represent  $\mathbf{Z}^+$  for the first  $e^+$  bunch  $e_1^+$  at a particular instant of time. One-third of a turn later, this bunch has moved to  $\text{IP}_2$  and is represented by  $\mathbf{Y}_2$ , while the third  $e^+$  bunch  $e_3^+$  has moved from  $\text{IP}_3$  to  $\text{IP}_1$  and is now represented by  $\mathbf{Y}_1$ . The  $e^+$  bunches pass through  $\text{IP}_1$  in the order 1, 3, 2, through  $\text{IP}_2$  in the order 2, 1, 3, and through  $\text{IP}_3$  in the order 3, 2, 1. Similarly, the  $e^-$  bunches pass through  $\text{IP}_1$  in the order 1, 2, 3, through  $\text{IP}_2$  in the order 2, 3, 1, and through  $\text{IP}_3$  in the order 3, 1, 2. The correspondence between state vectors  $\mathbf{Y}_i$  and  $e^\pm$  bunch numbers for three successive collisions is shown in Table I.

The cyclic permutation of the  $e^-$  bunches from (1, 2, 3) to (2, 3, 1) is described by the  $6 \times 6$  matrix  $P$ :

$$P = \begin{pmatrix} O & I & O \\ O & O & I \\ I & O & O \end{pmatrix}. \quad (9)$$





TABLE II Mode coupling pattern of  $M_{\sigma\pi}$  for the  $3 \oplus 3 = 3$  case. The type  $-$ ,  $+$  and  $c$  refers to negative, positive and complex eigenvalues

<i>Encounter</i>	<i>Unstable region</i>	<i>Type</i>
$\lambda_+$ vs. $\lambda_+^*$	$\nu_+ \lesssim 1/2$	$-$
	$\nu_+ \lesssim 1$	$+$
$\lambda_-$ vs. $\lambda_-^*$	$\nu_- \lesssim 1/2$	$-$
	$\nu_- \lesssim 1$	$+$
$\lambda_+$ vs. $\lambda_-^*$	$\nu_+ + \nu_- \lesssim \text{integer} / 2$	$c$
$\lambda_-$ vs. $\lambda_+^*$		$c$

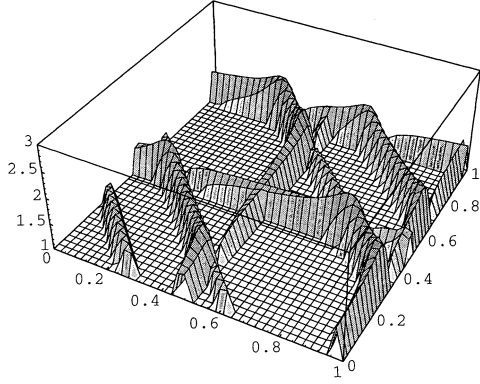
As  $\Xi$  grows, the eigenvalues move on the unit circle until two of them meet. We have observed that then one of the eigenvalues  $\lambda$  of the matrix  $M_{\sigma\pi}$  becomes larger than unity in absolute value. We summarize the mode coupling pattern in Table II.

When  $\lambda$  is an eigenvalue of  $M_\chi$ ,  $\lambda^*$  is an eigenvalue of  $M_{\chi^*}$ , and vice versa. Thus only  $M_\chi$  or  $M_{\chi^*}$  needs to be studied. Also for the discussion of  $M_\chi$ , we start with  $\Xi \ll 1$  where the eigenvalues of  $M_\chi$  are:

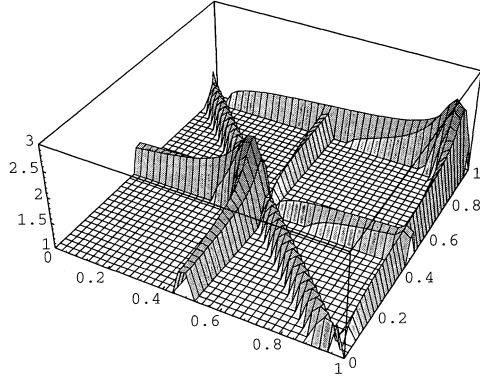
$$\begin{aligned}
 \lambda_1 &\approx \exp[2\pi i(+1/3 + \nu_+ + \Xi)] , \\
 \lambda_2 &\approx \exp[2\pi i(+1/3 - \nu_+ - \Xi)] , \\
 \lambda_3 &\approx \exp[2\pi i(-1/3 + \nu_- + \Xi)] , \\
 \lambda_4 &\approx \exp[2\pi i(-1/3 - \nu_- - \Xi)] .
 \end{aligned}
 \tag{22}$$

As  $\Xi$  grows, the eigenvalues move on the unit circle until two of them meet. We have observed numerically that then one of the eigenvalues  $\lambda$  of the matrix  $M_\chi$  becomes larger than unity in absolute value. All possible encounters of the eigenvalues and corresponding instabilities can thus be understood and are shown in Table III. The unstable regions of  $M_\chi^3$ ,  $M_{\sigma\pi}^3$  and  $M_1$  are compared in Figure 2. We can limit the ranges of  $\nu_+$  and  $\nu_-$  because (13) shows that  $U_\pm$  is invariant to a change of  $\nu_\pm$  by one unit. Furthermore, a simultaneous change  $\nu_+ \rightarrow \nu_+ \pm 1/2$  and  $\nu_- \rightarrow \nu_- \pm 1/2$  changes only the sign of  $\hat{U}$  but not the absolute values of the eigenvalues, resulting in the chessboard pattern. Figure 2 and Tables II and III summarize the  $3 \oplus 3 = 3$  case.

(A)



(B)



(C)

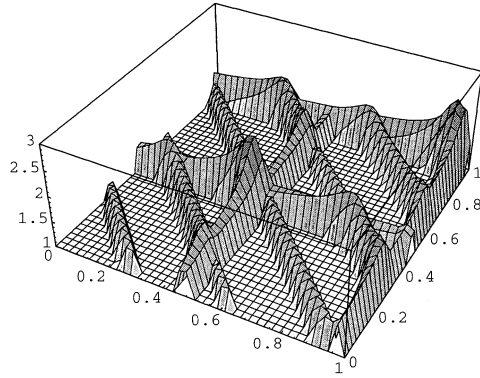


FIGURE 2 The largest absolute value of the eigenvalues of  $M_\chi^3$  (A),  $M_{\sigma\pi}^3$  (B) and  $M_1$  (C) as functions of  $(\nu_+, \nu_-) = (Q^+/3, Q^-/3)$  for the  $3 \oplus 3 = 3$  case with  $\Xi = 0.025$ .

TABLE III Mode coupling pattern of  $M_x$ . The type  $-$ ,  $+$  and  $c$  refers to negative, positive and complex eigenvalues for  $M_x^3$

<i>Encounter</i>	<i>Unstable region</i>	<i>Type</i>
$\lambda_1$ vs. $\lambda_2$	$\nu_+ \lesssim 1/2$ $\nu_+ \lesssim 1$	$-$ $+$
$\lambda_3$ vs. $\lambda_4$	$\nu_- \lesssim 1/2$ $\nu_- \lesssim 1$	$-$ $+$
$\lambda_1$ vs. $\lambda_4$	$\nu_+ + \nu_- \lesssim 1/3$ $\nu_+ + \nu_- \lesssim 4/3$	$c$ $c$
$\lambda_2$ vs. $\lambda_3$	$\nu_+ + \nu_- \lesssim 2/3$ $\nu_+ + \nu_- \lesssim 5/3$	$c$ $c$

### 3.2 The $3 \oplus 3 = 6$ Case

This case is the simplest non-trivial  $N \oplus N = 2N$  case. We add three primed IPs, labelled  $IP'_1$ ,  $IP'_2$  and  $IP'_3$  to the IPs of the  $3 \oplus 3 = 3$  case, such that primed and unprimed IPs alternate. Let all bunches collide at the unprimed IPs at a particular instant of time. They will then collide at the primed IPs one collision later. We still use the state vectors  $\mathbf{Y}$  for the unprimed IPs. For the primed IPs, we define new state vectors  $\mathbf{W} = (\mathbf{W}_1, \mathbf{W}_2, \dots, \mathbf{W}_6)^t$ , where,

$$\begin{aligned} \mathbf{W}_1 &: e^+ \text{ at } IP'_1 & \mathbf{W}_4 &: e^- \text{ at } IP'_1 \\ \mathbf{W}_2 &: e^+ \text{ at } IP'_2 & \mathbf{W}_5 &: e^- \text{ at } IP'_2 \\ \mathbf{W}_3 &: e^+ \text{ at } IP'_3 & \mathbf{W}_6 &: e^- \text{ at } IP'_3. \end{aligned}$$

The correspondence between state vectors  $\mathbf{W}_i$  and  $\mathbf{Y}_i$  and  $e^\pm$  bunch numbers for six successive collisions is shown in Table IV.

TABLE IV Correspondence between state vectors  $\mathbf{W}_i$  and  $\mathbf{Y}_i$  and  $e^\pm$  bunches for six successive instants  $i$  during a turn in the  $3 \oplus 3 = 6$  case

$i$	$\mathbf{Y}_1$	$\mathbf{Y}_2$	$\mathbf{Y}_3$	$\mathbf{Y}_4$	$\mathbf{Y}_5$	$\mathbf{Y}_6$	$\mathbf{W}_1$	$\mathbf{W}_2$	$\mathbf{W}_3$	$\mathbf{W}_4$	$\mathbf{W}_5$	$\mathbf{W}_6$
1	$e_1^+$	$e_2^+$	$e_3^+$	$e_1^-$	$e_2^-$	$e_3^-$						
2							$e_1^+$	$e_2^+$	$e_3^+$	$e_1^-$	$e_2^-$	$e_3^-$
3	$e_3^+$	$e_1^+$	$e_2^+$	$e_2^-$	$e_3^-$	$e_1^-$						
4							$e_3^+$	$e_1^+$	$e_2^+$	$e_2^-$	$e_3^-$	$e_1^-$
5	$e_2^+$	$e_3^+$	$e_1^+$	$e_3^-$	$e_1^-$	$e_2^-$						
6							$e_2^+$	$e_3^+$	$e_1^+$	$e_3^-$	$e_1^-$	$e_2^-$

The  $\mathbf{W}$  is related to the  $\mathbf{Y}$  at the previous collision by

$$\mathbf{W} = \begin{pmatrix} I & O \\ O & P \end{pmatrix} \hat{U} R \mathbf{Y}_{\text{previous}} . \quad (23)$$

This  $\mathbf{W}$  is related to the next  $\mathbf{Y}$  by

$$\mathbf{Y}_{\text{new}} = \begin{pmatrix} P^2 & O \\ O & I \end{pmatrix} \hat{U} R \mathbf{W} . \quad (24)$$

Thus, we have

$$M_1 = M_{1/3}^3, \quad M_{1/3} = \begin{pmatrix} P^2 & O \\ O & I \end{pmatrix} \hat{U} R \begin{pmatrix} I & O \\ O & P \end{pmatrix} \hat{U} R . \quad (25)$$

As before, by multiplying with  $\text{diag}(V, V^\dagger)$  from the left and with  $\text{diag}(V^\dagger, V)$  from the right and by reordering the basis vectors, we have three mutually decoupled systems:

$$M_{1/3} \sim \text{diag} \left[ M_{\sigma\pi}^2, M_{\chi^{1/2}}^2, M_{\chi^{1/2*}}^2 \right] . \quad (26)$$

Here  $M_{\sigma\pi}$  is defined by (19), and  $M_{\chi^{1/2}}$  is the same as that defined by (20) but  $\chi$  is replaced by  $\chi^{1/2} = \exp(\pi i/3)$ . We thus arrive at

$$M_1 \sim \text{diag} \left[ M_{\sigma\pi}^6, M_{\chi^{1/2}}^6, M_{\chi^{1/2*}}^6 \right] . \quad (27)$$

For  $\mathfrak{E} \ll 1$ , the eigenvalues of  $M_{\chi^{1/2}}$  can be predicted as shown in (22) with  $1/3$  replaced by  $1/6$ . Table III also applies to the  $3 \oplus 3 = 6$  case if we interchange “ $\lambda_1$  vs.  $\lambda_4$ ” and “ $\lambda_2$  vs.  $\lambda_3$ ”.

Thus we conclude that, in the  $(\nu_+, \nu_-)$ -plane, the  $3 \oplus 3 = 6$  case has exactly the same instability pattern as the  $3 \oplus 3 = 3$  case in Tables II and III. We will show in Section 3.5 that this is not an accident. In the  $(Q^+, Q^-)$ -plane, the resonances are twice as far apart, compared to the  $3 \oplus 3 = 3$  case.

### 3.3 The $N \oplus N = N$ Case

For the discussion of the  $N \oplus N = N$  case, we can restrict ourselves to the case where  $N$  is odd. It follows from the family theorem in Appendix A that the  $N \oplus N = N$  case is irreducible when  $N$  is odd. When  $N$  is even, the  $N \oplus N = N$  case splits into two mutually independent and identical  $N/2 \oplus N/2 = N$  cases with the same eigenvalues. The latter case will be studied later when we discuss the  $N \oplus N = 2N$  case.

As before, we define the state vector  $\mathbf{Y} = (\mathbf{Y}_1, \dots, \mathbf{Y}_{2N})^t$ , where  $\mathbf{Y}_i$  denotes the state vector of the  $e^+$  bunch at the  $i$ -th IP and  $\mathbf{Y}_{N+i}$  that of the  $e^-$  bunch at the  $i$ -th IP ( $i = 1, 2, \dots, N$ ). With  $\chi_N \equiv \exp(2\pi i/N)$ , the matrices  $P$  in (9) and  $V$  in (15) are replaced by

$$P = \begin{pmatrix} O & I & O & \dots & O \\ \vdots & O & \ddots & \ddots & \vdots \\ \vdots & O & O & \ddots & O \\ O & O & O & O & I \\ I & O & \dots & \dots & O \end{pmatrix}, \quad (28)$$

$$V = \frac{1}{\sqrt{N}} \begin{pmatrix} I & I & I & \dots & I \\ I & \chi_N I & \chi_N^2 I & \dots & \chi_N^{N-1} I \\ I & \chi_N^2 I & \chi_N^4 I & \dots & \chi_N^{2(N-1)} I \\ \vdots & \vdots & \vdots & \vdots & \vdots \\ I & \chi_N^{N-1} I & \chi_N^{2(N-1)} I & \dots & \chi_N^{(N-1)^2} I \end{pmatrix}. \quad (29)$$

Then we have  $M_1 \sim M_{1/N}^N$ , where

$$M_{1/N} \sim \text{diag} [m(0), m(1/N), m(-1/N), \dots, m(n/N), m(-n/N), \dots, m((N-1)/(2N)), m(-(N-1)/(2N))]. \quad (30)$$

Here  $m(n/N)$  is the same as  $M_\chi$  (20), with  $\chi = \exp(2\pi i n/N)$ , and  $m(0)$  is identical to  $M_{\sigma\pi}$  (19). Clearly,  $m(n/N)$  and  $m(-n/N)$  have the same instability property. The generalization of (22) to  $m(n/N)$  for  $\Xi \ll 1$  yields:

$$\begin{aligned} \lambda_1 &\approx \exp[2\pi i(+n/N + \nu_+ + \Xi)], \\ \lambda_2 &\approx \exp[2\pi i(+n/N - \nu_+ - \Xi)], \\ \lambda_3 &\approx \exp[2\pi i(-n/N + \nu_- + \Xi)], \\ \lambda_4 &\approx \exp[2\pi i(-n/N - \nu_- - \Xi)]. \end{aligned} \quad (31)$$

Note that  $n/N = 1/2$  never happens because  $N$  is odd. Also note that we can assume  $0 \leq n < N/2$  without losing generality. All mode-coupling patterns for the  $N \oplus N = N$  case are listed in Table V.

TABLE V Mode coupling pattern of  $m(n/N)$  for the  $N \oplus N = N$  case. Note that  $\nu_{\pm} = Q^{\pm}/N \pmod{1}$ . The type  $-$ ,  $+$  and  $c$  refers to the negative, positive and complex eigenvalues for  $m(n/N)^N$ . We have  $0 \leq n < N/2$ . The case  $n = 0$  corresponds to  $M_{\sigma\pi}$

<i>Encounter</i>	<i>Unstable region</i>	<i>Type</i>
$\lambda_1$ vs. $\lambda_2$	$\nu_+ \lesssim 1/2$	$-$
	$\nu_+ \lesssim 1$	$+$
$\lambda_3$ vs. $\lambda_4$	$\nu_- \lesssim 1/2$	$-$
	$\nu_- \lesssim 1$	$+$
$\lambda_1$ vs. $\lambda_4$	$\nu_+ + \nu_- \lesssim (N - 2n)/N$	$c$
	$\nu_+ + \nu_- \lesssim 2(N - n)/N$	$c$
$\lambda_2$ vs. $\lambda_3$	$\nu_+ + \nu_- \lesssim 2n/N$	$c$
	$\nu_+ + \nu_- \lesssim (N + 2n)/N$	$c$

### 3.4 The $N \oplus N = 2N$ Case

In the general  $N \oplus N = 2N$  case,  $N$  can either be odd or even. Both cases are irreducible. By the same transformations as before, using  $\text{diag}(V, V^{\dagger})$  with  $V$  defined by (29) and  $\chi = \exp(2\pi i/N)$  as before, we get

$$M_1 = M_{1/(2N)}^{2N}, \quad (32)$$

where

$$\begin{aligned} M_{1/(2N)} \sim & \text{diag} [m(0), m(1/(2N)), m(-1/(2N)), \\ & \dots, m(n/(2N)), m(-n/(2N)), \\ & \dots, m((N-1)/(4N)), m(-(N-1)/(4N))] \quad (N \text{ odd}) \end{aligned} \quad (33)$$

$$\begin{aligned} M_{1/(2N)} \sim & \text{diag} [m(0), m(1/(2N)), m(-1/(2N)), \\ & \dots, m(n/(2N)), m(-n/(2N)), \\ & \dots, m((N-2)/(4N)), m(-(N-2)/(4N)), m(1/4)] \quad (N \text{ even}) \end{aligned} \quad (34)$$

TABLE VI Mode-coupling pattern of  $m(n/(2N))$ . Note that  $v_{\pm} = Q^{\pm}/(2N) \pmod{1}$ . For the  $N \oplus N = 2N$  case, the type  $-$ ,  $+$  and  $c$  refers to the negative, positive and complex eigenvalues for  $m(n/(2N))^{2N}$ . We have  $0 \leq n \leq N/2$

<i>Encounter</i>	<i>Unstable region</i>	<i>Type</i>
$\lambda_1$ vs. $\lambda_2$	$v_+ \lesssim 1/2$	$+$
	$v_+ \lesssim 1$	$+$
$\lambda_3$ vs. $\lambda_4$	$v_- \lesssim 1/2$	$+$
	$v_- \lesssim 1$	$+$
$\lambda_1$ vs. $\lambda_4$	$v_+ + v_- \lesssim (N - n)/N$	$c$
	$v_+ + v_- \lesssim (2N - n)/N$	$c$
$\lambda_2$ vs. $\lambda_3$	$v_+ + v_- \lesssim n/N$	$c$
	$v_+ + v_- \lesssim (N + n)/N$	$c$

For  $\Xi \ll 1$ , the eigenvalues of  $m(n/(2N))$  are

$$\begin{aligned}
 \lambda_1 &\approx \exp[2\pi i(+n/(2N) + v_+ + \Xi)] \\
 \lambda_2 &\approx \exp[2\pi i(+n/(2N) - v_+ - \Xi)] \\
 \lambda_3 &\approx \exp[2\pi i(-n/(2N) + v_- + \Xi)] \\
 \lambda_4 &\approx \exp[2\pi i(-n/(2N) - v_- - \Xi)]
 \end{aligned} \tag{35}$$

Here  $0 \leq n \leq N/2$  is assumed and the  $n = 0$  case corresponds to  $M_{\sigma\pi}$ . The case  $n = N/2$  occurs only when  $N$  is even. Table VI shows the types of the unstable regions, and Figure 3 the schematic instability lines.

### 3.5 Equivalence of $N \oplus N = N$ and $N \oplus N = 2N$ Cases for Odd $N$

So far, we have examined the cases  $N \oplus N = N$  for odd  $N$  and  $N \oplus N = 2N$  for arbitrary  $N$ , and we show in the Appendix A that they are the only irreducible cases for equally spaced bunches and interaction points. We now show that the  $N \oplus N = N$  and  $N \oplus N = 2N$  cases are equivalent when  $N$  is odd. We observe that there are identical terms for even  $n$  in Equations (30) and (33). For odd  $n$ , we use  $m(\omega) = -m(\omega \pm 1/2)$ , and change the typical term in (33) as follows:

$$m\left(\frac{n}{2N}\right) = -m\left(\frac{n}{2N} + \frac{1}{2}\right) = -m\left(-\frac{N-n}{2N}\right). \tag{36}$$

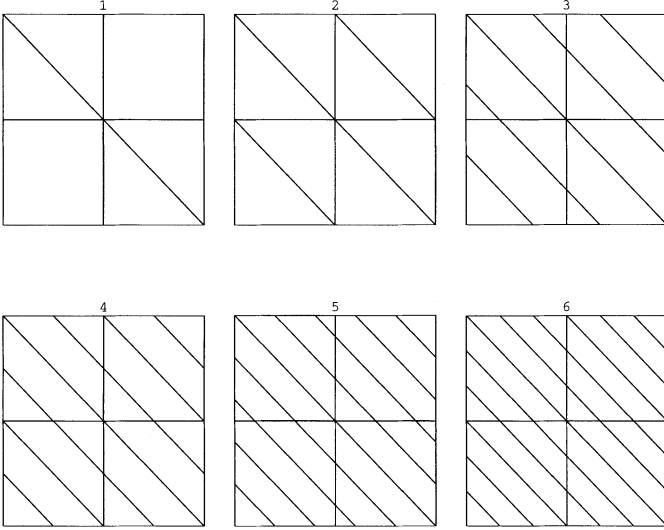


FIGURE 3 The edges of the unstable region in  $(\nu_+, \nu_-)$  plane for  $0 \leq \nu_{\pm} \leq 1$ . For the  $N \oplus N = 2N$  case, these graphs can be taken as graphs in the  $(Q^+, Q^-)$ -plane for  $0 \leq Q^{\pm} \pmod{2N} \leq 2N$ . For the  $N \oplus N = N$  case with odd  $N$ , they can be used in the  $(Q^+, Q^-)$ -plane for  $0 \leq Q^{\pm} \pmod{N} \leq N$ .  $N$  is indicated in each graph.

We then notice that the modified terms in (33) are identical to the remaining terms in (30), apart from the sign which is irrelevant for the stability. Hence, we have demonstrated that, apart from the sign, the matrices

$$M_{1/N}(N \oplus N = N) \sim M_{1/(2N)}(N \oplus N = 2N), \quad (37)$$

are equivalent, i.e. have the same absolute eigenvalues when  $N$  is odd. Therefore, the graphs in Figure 3 can be used both for  $N \oplus N = N$  cases with odd  $N$  and  $N \oplus N = 2N$  cases.

### 3.6 The $N \oplus N = N_{\text{IP}}$ Case for Arbitrary $N_{\text{IP}}$

We now consider the case of equally spaced bunches and IPs for arbitrary  $N \oplus N = N_{\text{IP}}$ , such that  $N_{\text{IP}}$  is an integral fraction of  $2N$ . The algorithm for reducing  $N$  is as follows:

1. calculate the number of families  $N_F = \gcd(N, 2N/N_{IP})$ , (see Appendix A),
2. reduce the  $N \oplus N = N_{IP}$  case to the  $N/N_F \oplus N/N_F = N_{IP}$  case, arriving at either  $N' \oplus N' = N'$  ( $N'$  odd) or at  $N' \oplus N' = 2N'$  for  $N' = N/N_F$ , which are both irreducible,
3. find a graph in Figure 3 with index  $N'$ , which shows the unstable region in the  $(Q^+, Q^-)$ -plane for  $0 \leq Q^\pm \pmod{N_{IP}} \leq N_{IP}$ .

Let us consider cases with  $N = 6$  and all possible values of  $N_{IP}$ , starting at the highest value  $N_{IP} = 12$ , and taking all values which are divisors of 12, as shown in Table VII. For example, we find the instability pattern of the  $6 \oplus 6 = 3$  case by looking at the index 3 in Figure 3 where both axes are from 0 to 3 in  $Q^\pm$ .

TABLE VII Table of all possible cases for 6 bunches in each beam

$N \oplus N = N_{IP}$	$S$	$N_F$	$N'$	<i>reduced case</i>
$6 \oplus 6 = 12$	1	1	6	irreducible
$6 \oplus 6 = 6$	2	2	3	$3 \oplus 3 = 6$
$6 \oplus 6 = 4$	3	3	2	$2 \oplus 2 = 4$
$6 \oplus 6 = 3$	4	2	3	$3 \oplus 3 = 3$
$6 \oplus 6 = 2$	6	6	1	$1 \oplus 1 = 2$
$6 \oplus 6 = 1$	12	6	1	$1 \oplus 1 = 1$

### 3.7 Instability Threshold for Equal Tunes

In all  $N \oplus N = N_{IP}$  cases, where  $\nu_+ = \nu_- \equiv \nu$  holds in addition to  $\Xi^+ = \Xi^- \equiv \Xi$ , we can analytically calculate the threshold of the instability, i.e. the minimum value of  $\Xi$  that gives the instability.

The instability threshold  $\hat{\Xi}_{\sigma\pi}$  for the  $M_{\sigma\pi}$  block, (19), is well known. Applying a similarity transformation, we can reduce  $M_{\sigma\pi}$  to blockwise diagonal form:

$$\begin{aligned}
 M_{\sigma\pi} &\sim T\hat{U}(\nu)TTR(\Xi, \Xi)T \sim \hat{U}(\nu) \begin{pmatrix} I & O \\ O & I - 2A \end{pmatrix} \\
 &\sim \begin{pmatrix} U(\nu) & O \\ O & U(\nu)(I - 2A) \end{pmatrix}
 \end{aligned} \tag{38}$$

where  $U$  is defined by (2) and  $T$  is the symplectic  $4 \times 4$  matrix

$$T = \frac{1}{\sqrt{2}} \begin{pmatrix} I & I \\ I & -I \end{pmatrix}, \quad (39)$$

which satisfies  $T^2 = I$ . The upper half of (38) corresponds to the so-called  $\sigma$  mode whose tune is not shifted by the beam-beam interaction. The lower half is the  $\pi$  mode. Its perturbed tune  $\nu_\pi$  is

$$\cos 2\pi \nu_\pi = \cos 2\pi \nu - 4\pi \Xi \sin 2\pi \nu, \quad (40)$$

which can also be derived from (8). For  $\Xi \ll 1$ ,  $\nu_\pi \approx \nu + 2\Xi$ . The  $\pi$  mode becomes unstable if and only if  $\cos 2\pi \nu_\pi$  becomes  $\pm 1$ . Solving (40) with this condition yields for the instability threshold

$$\hat{\Xi}_{\sigma\pi} = \frac{\cos 2\pi \nu \mp 1}{4\pi \sin 2\pi \nu}. \quad (41)$$

The  $\hat{\Xi}_{\sigma\pi}$  is shown in the graph in Figure 4, labelled 1.

To find the threshold  $\hat{\Xi}_\chi$  of the  $M_\chi$  block, (20), for arbitrary  $\chi$ , explicit expressions for the eigenvalues are not needed, because we know from Tables V and VI that the instability develops if and only if an eigenvalue  $\lambda$  becomes  $\pm 1$ . The eigenvalue equation for  $M_\chi$  yields:

$$\Xi = \frac{(1 - 2\lambda\chi \cos 2\pi \nu + \lambda^2 \chi^2)(\chi^2 + \lambda^2 - 2\lambda\chi \cos 2\pi \nu)}{(4\pi \lambda \chi \sin 2\pi \nu)[4\lambda\chi \cos 2\pi \nu - (\lambda^2 + 1)(\chi^2 + 1)]}, \quad (42)$$

Hence, we find the threshold for arbitrary  $\chi$  by substituting  $\lambda = \pm 1$ :

$$\hat{\Xi}_\chi = \frac{\cos 2\pi \nu \mp \cos 2\pi \omega}{4\pi \sin 2\pi \nu}, \quad (43)$$

Here  $\chi = \exp(2\pi i \omega)$ . When  $\omega = 0$ , this equation is identical to (41).

In order to obtain the instability threshold  $\hat{\Xi}$  for the one-turn map  $M_1$  of the  $N \oplus N = N_{\text{IP}}$  case we first find the irreducible  $N' \oplus N' = N_{\text{IP}}$  case, cf. Section 3.6. Then we evaluate (43) for all values of  $\omega$  appearing in Equations (33) and (34), and obtain the smallest positive  $\hat{\Xi}_\chi$  which is  $\hat{\Xi}$ . Since we know the branch which leads to the lowest value of  $\hat{\Xi}$ , we can avoid looking for the minimum  $\hat{\Xi}_\chi$ , and find:

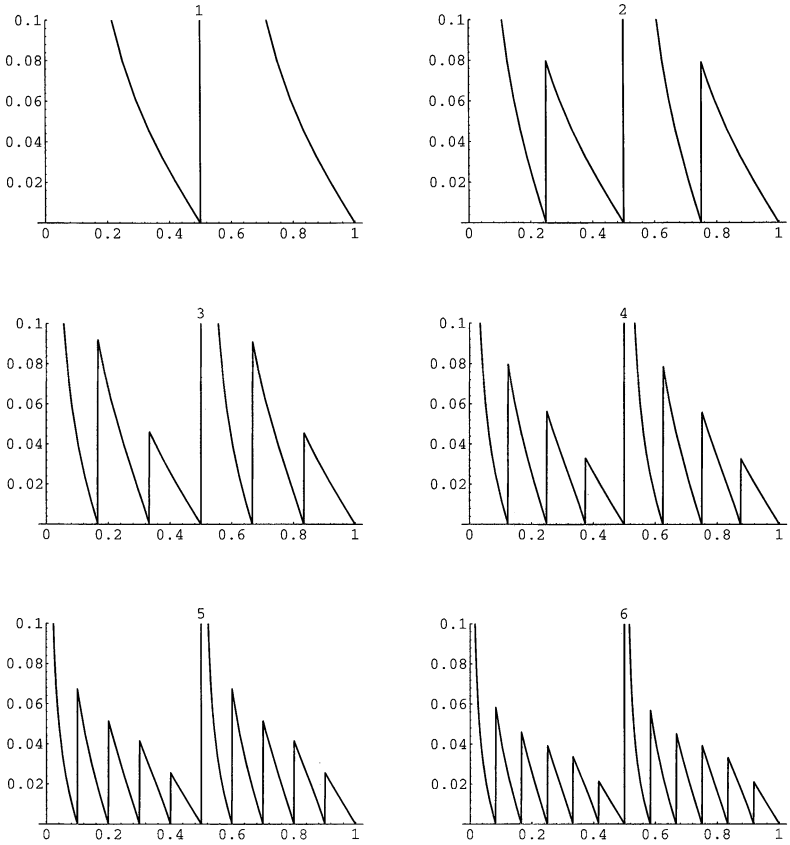


FIGURE 4 The threshold value of  $\hat{\Xi}$  for  $N \oplus N = 2N$  cases as a function of  $\nu$ . The  $N$  is indicated in the graph. Each graph gives the  $\hat{\Xi}$  for the case given in Figure 3 with the same index. It is thus also usable for general cases if  $N$  in the graph is interpreted as  $N' = N/N_{\text{IP}}$  and the horizontal axis as  $Q$  (modulo  $N_{\text{IP}}$ ) from 0 to  $N_{\text{IP}}$ .

$$\hat{\Xi} = \frac{\cos\{2\pi Q/N_{\text{IP}}\} - \cos\{2\pi([Q+1]/N_{\text{IP}})\}}{4\pi \sin\{2\pi Q/N_{\text{IP}}\}}. \quad (44)$$

Here we use the tune  $Q \equiv N_{\text{IP}} \nu$ , and  $[a]$  is the largest positive integer that does not exceed  $a$ . The value of  $\hat{\Xi}$  given by (44) is shown as a function of  $\nu$  in Figure 4 with  $1 \leq N \leq 6$  as a parameter. The graphs are valid both for  $N' \oplus N' = N'$  with odd  $N'$  and  $N' \oplus N' = 2N'$  cases. The horizontal axes can also be taken as  $0 \leq Q \pmod{N_{\text{IP}}} \leq N_{\text{IP}}$ .

Piwinski's result<sup>12</sup> applies to the  $N \oplus N = 2N$  case and looks similar but is different even in this case in two important respects: (i) Piwinski finds resonances at half-integral values of  $Q$  which do not exist, (ii) a factor of two is caused by the ratio of  $\Xi$  and  $\xi$ . Our result applies to all  $N \oplus N = N_{\text{IP}}$  cases.

It is interesting to note that the threshold  $\hat{\Xi}$  can be obtained by requiring that the  $\pi$  mode eigenvalues of  $M_1$  become  $\pm 1$ , although it is not always the  $\pi$  mode which causes the instability. (The eigenvalue can pass  $\pm 1$  along the unit circle without causing instability.) This is so because (42) is symmetric in  $\chi$  and  $\lambda$ , and therefore the eigenvalue  $\lambda_\pi$  of  $M_{\sigma\pi}$  becomes  $\pm \exp(2\pi i\omega)$  when the eigenvalue  $\lambda_\omega$  of  $M_\chi$  becomes  $\pm 1$ . Thus, (43) can also be derived by putting  $\cos 2\pi\nu_\pi = \pm \cos \omega$  into (40).

### 3.8 Summary for Perfect Machines

We have studied the coherent beam-beam effects in the framework of the LRGM where we consider only the linear focusing force between the barycentres of two bunches colliding head-on. The dominant effect in this case is a change of focusing, parametrized by the beam-beam strength parameter  $\Xi$ . We study the stability of the motion of the barycentres using the eigenvalues of the one-turn map. We call the case of  $N$  electron bunches colliding with  $N$  positron bunches in  $N_{\text{IP}}$  interaction points  $N \oplus N = N_{\text{IP}}$ , and give closed analytical solutions for it.

In Section 3.6, we give the algorithm for finding the irreducible  $N' \oplus N' = N_{\text{IP}}$  case for the arbitrary  $N \oplus N = N_{\text{IP}}$  case. All irreducible cases are either  $N \oplus N = N$  with odd  $N$  or  $N \oplus N = 2N$ . Furthermore, these two cases show exactly the same instability patterns in the  $(Q^+, Q^-)$ -plane. The period of the resonances in  $Q^\pm$  is  $N$  for the  $N \oplus N = N$  case with odd  $N$ , and  $2N$  for the  $N \oplus N = 2N$  case with odd  $N$ , and the  $(Q^+, Q^-)$ -plane is filled in a chess board pattern. In all cases with even  $N$ , the period in  $Q^\pm$  is  $N$ , and the resonance pattern repeats itself in the  $(Q^+, Q^-)$ -plane every  $N$  units of tune. For all cases, the edges of the resonances in tune space can be found in Figure 3. The case with equal tunes,  $Q^+ = Q^-$ , corresponds to the diagonal from lower left to upper right, the threshold is given by (44) and is found in Figure 4.

## 4 MACHINES WITH ERRORS

We have neglected up to now the errors in real machines which occur there for several reasons:

1. The currents of the bunches in the two beams are not exactly equal.
2. The betatron functions  $\alpha$  and  $\beta$  differ from IP to IP and between the two beams.
3. The phase advances  $\mu$  between IPs differ from arc to arc and between the two beams.
4. Electrons and positrons have different energies at all IPs because of asymmetries of the RF accelerations between the IPs, either by design or by errors in the RF system.<sup>27</sup>
5. The emittances of the two beams are different.

In this section, we present the results of numerical computations of the consequences of these errors, which cause  $N \oplus N = 2N$  machines with errors to behave to a large extent like  $1 \oplus 1 = 1$  machines. In particular, the half-integral resonances appear, and the complex sum resonances occur when the sum of the tunes in the two beams is just below an integer. We have already discussed errors in  $1 \oplus 1 = 1$  machines in Section 2.

#### 4.1 $1 \oplus 1 = 2$ Machines with Errors

We simultaneously put errors on the phase advances  $v_i^\pm = Q^\pm/2 + \delta v_\pm r$ , bunch currents  $I_i^\pm = I + \delta I^\pm r$ , and  $\beta$ -functions  $\beta_{xi}^\pm = \beta_{xi}^\pm + \delta\beta_x^\pm r$ ,  $\beta_{yi}^\pm = \beta_{yi}^\pm + \delta\beta_y^\pm r$ , where the  $r$ 's are all independent random Gaussian variables with zero average and unit variance. In Figure 5 we show the average growth rates in the  $(Q^+, Q^-)$ -plane for ten sets of random errors. The excitation of the error-driven resonances depends strongly on the random errors, while the resonances already present in the perfect machine remain about the same. In contrast to the perfect  $1 \oplus 1 = 2$  machine, the errors cause the following error-driven resonances: (i) half-integral resonances when either  $Q^+$  or  $Q^-$  is equal to an integer and one-half, (ii) complex sum resonances when the sum of the tunes ( $Q^+ + Q^-$ ) is just below an integer. These resonances are already present in perfect  $1 \oplus 1 = 1$  machines. Figure 5 shows that the histogram channels just below the integral and half-integral tunes are filled with the integral and half-integral resonances. Hence, the upper edge of these resonances coincides with the exact integral or half-integral tunes within the accuracy of the histograms. However, the upper edge of the error-driven sum resonances is one channel or more below the integral value of the sum ( $Q^+ + Q^-$ ). We will come across other examples of this shifting of error-driven sum resonances later, and believe that it is





now twice as large, and the number of resonances in  $Q^+$  or  $Q^-$  is four times as large. The increased number of resonances divides the  $(Q^+, Q^-)$ -plane into much smaller pieces, and reduces the fraction not covered by resonances from 0.696 to  $0.582 \pm 0.045$ .

### 4.3 Machines with $N \geq 3$

Further numerical studies with random errors on the bunch currents, phase advances and  $\beta$ -functions at the IP, in both  $N \oplus N = N$  for  $N = 3$  and  $N \oplus N = 2N$  cases with  $N = 3, 4$ , show that resonances occur when  $Q^\pm \pmod{1} \lesssim 1/2$ ,  $Q^\pm \pmod{1} \lesssim 1$ , and  $(Q^+ + Q^-) \pmod{1} \lesssim 1$ , i.e. at the same tunes where resonances occur in the  $1 \oplus 1 = 1$  case. Figure 7 shows the  $3 \oplus 3 = 3$  case as an example. Compared to the perfect  $N \oplus N = N$  case with odd  $N$ , the number of resonances in  $Q^\pm$  increases by a factor of  $N$ , and the number of sum resonances remains the same. Compared to the perfect  $N \oplus N = 2N$  case with any  $N$ , the number of resonances in  $Q^\pm$  increases by a factor of  $2N$ , and the number of sum resonances doubles. The periodicity of the resonances in the  $(Q^+, Q^-)$ -plane is the same as in perfect machines, discussed in Section 3.8.

## 5 DISCUSSION OF COMPLEX RESONANCES

In this section, we first calculate analytically the complex resonances for the  $1 \oplus 1 = 2$  case which are excited by the differences of the phase advances in the arcs. Next we discuss LEP, where the separation in half of the interaction points is not so large that the beam-beam tune shifts can be neglected completely.

### 5.1 Complex Resonances in Asymmetric $1 \oplus 1 = 2$ Machines

Chao and Keil<sup>13</sup> studied the case of a conventional single-ring machine where the phase advances of the  $e^+$  and the  $e^-$  beams are identical in the same arc,  $\nu_1^+ = \nu_1^- \equiv Q/2 + \delta$  and  $\nu_2^+ = \nu_2^- \equiv Q/2 - \delta$ , with  $\delta \neq 0$ , and where all  $\Xi_{1,2}^\pm = \Xi$  are identical. We use this case for a demonstration of the behaviour of the complex resonances. The one-turn matrix  $M_1$  is:

$$M_1 = \hat{U}(Q/2 + \delta, Q/2 - \delta)R(\Xi, \Xi)\hat{U}(Q/2 - \delta, Q/2 + \delta)R(\Xi, \Xi). \quad (45)$$



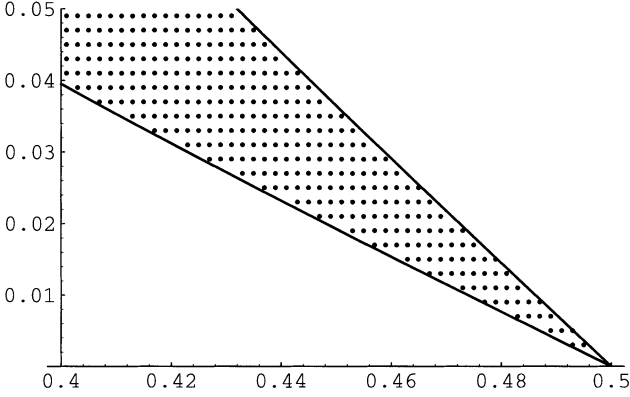


FIGURE 8 Half-integral stopband in a  $1 \oplus 1 = 2$  machine with phase advances  $2\pi(Q/2+0.1)$  and  $2\pi(Q/2-0.1)$ . The abscissa is the tune  $Q$ , the ordinate is  $\Xi$ .

where  $a = 4\pi \Xi$ . The complex resonance with  $D < 0$  can only occur when the phases in the two arcs are different, i.e.  $\delta \neq 0$  holds. It is centred where the first term in the square bracket of  $D$  vanishes, at  $\Xi = (1/2\pi) \cot \pi Q$ , i.e. at  $Q < 1/2$  for attractive beam-beam forces with  $a > 0$ . Its width in the  $\Xi$  direction is determined by the second term in the square bracket for  $D$ :

$$\frac{\cot \pi Q}{2\pi(1 + |\sin \pi \delta|)} < \Xi < \frac{\cot \pi Q}{2\pi(1 - |\sin \pi \delta|)}. \quad (48)$$

The region of instability in the  $(Q, \Xi)$ -plane is shown in Figure 8. For small  $\Xi$ , the instability occupies a small range of  $Q$  just below  $Q = 0.5$ . With increasing  $\Xi$ , the instability becomes wider and shifts towards smaller values of  $Q$ . For a fixed value of  $Q < 1/2$ , the instability occupies a range of  $\Xi$  values, with stability above and below this range.

Another simple case is that of  $\text{DA}\Phi\text{NE}^{28,29}$  which has two rings, each consisting of two rather different arcs with phase advances  $2\pi(Q/2 + \delta)$  and  $2\pi(Q/2 - \delta)$ , respectively, and collisions in two interaction points. The revolution matrix is different from (45):

$$M = \hat{U}(Q/2 + \delta, Q/2 + \delta)R(\Xi, \Xi)\hat{U}(Q/2 - \delta, Q/2 - \delta)R(\Xi, \Xi). \quad (49)$$



The real parts of the eigenvalues are:

$$\begin{aligned}\cos \bar{\mu}_\sigma &= \cos 2\pi Q, \\ \cos \bar{\mu}_\pi &= \cos 2\pi Q - 2a \sin 2\pi Q + a^2 (\cos 4\pi\delta - \cos 2\pi Q).\end{aligned}\tag{50}$$

Hence, the tune of the  $\sigma$ -mode does not move,  $\cos \bar{\mu}_\pi$  is real, and the complex resonance does not occur.

In Figure 9 we show the instability region in the tune space for both cases. When moving along the diagonal line ( $\nu_+ = \nu_-$ ) in the left halves of Figures 9A and 9B, instability occurs at half-integers. It is of complex type for the conventional case (45), and of half-integral type for DAΦNE (49). If the phase advances in the arcs are different in the  $1 \oplus 1 = 2$  case, we can predict the existence but not the type of the instability originating at half-integral tunes.

Chao and Furman<sup>16,17</sup> used a tracking method for the beam-beam modes in the SSC where the interaction points are arranged in two different ‘clusters’. They found half-integral resonances of a characteristic sail shape very similar to our Figure 8. This result is not surprising, given the fact that the two halves of the SSC are different.

## 5.2 The LEP Case

In LEP, the two beams are vertically separated at the odd-numbered pits by about 3 mm. The beam radii there are  $\sigma_x \approx 0.57$  mm and  $\sigma_y \approx 50$   $\mu$ m. This separation is not quite enough to make the beam-beam focusing completely negligible. In both even- and odd-numbered pits in LEP, the ratio  $\beta_x/\beta_y \gg 1$ . Therefore, the ratio  $\Xi_x/\Xi_y \gg 1$  in the odd-numbered pits where the beams are separated, while in the even-numbered pits where the beams collide head-on, the ratio  $\Xi_x/\Xi_y \approx 1$ . Hence, the effects of the residual beam-beam tune shifts in the odd-numbered pits are stronger in the horizontal plane. When we apply our formalism to LEP, we are confronted with two difficulties:

1. The beam-beam force in the odd-numbered pits modifies the closed orbits of all bunches in both beams around the whole circumference of LEP.<sup>2</sup> We overcome this difficulty by assuming that the closed orbit in the even-numbered pits, where the head-on beam-beam collisions occur, is corrected locally by fine adjustments of the vertical electrostatic separators there, as is actually the case to optimize the luminosity.





forces between the barycentres of two bunches, assumed to be rigid bodies colliding head-on. The dominant effect in this case is a change of focusing, parametrized by the beam–beam strength parameter  $\Xi$ . We study the stability of the motion of the barycentres in linear approximation, using the eigenvalues of the one-turn map. We call the case of  $N$  equidistant electron bunches colliding with  $N$  equidistant positron bunches at  $N_{\text{IP}}$  equidistant interaction points  $N \oplus N = N_{\text{IP}}$ . In Section 3.6, we give the procedure which reduces the general case to its associated irreducible case. Figure 3 shows schematic diagrams of the resonances in perfect machines up to  $N = 6$ , while Figure 4 shows and (44) gives a closed expression for the threshold in terms of the coherent beam–beam parameter  $\Xi$  for the case of equal tunes in the two beams.

We find that errors in the machine, in particular in the bunch currents, the  $\beta$ -functions at the IPs and the phase advances through the arcs, which may be caused by the design or by inevitable errors in the construction, increase the number of beam–beam resonances. In machines with errors, integral resonances occur when one of the tunes  $Q^\pm \pmod{1} < 1$ , half-integral resonances occur when one of the tunes  $Q^\pm \pmod{1} < 1/2$ , and complex resonances occur when the sum of the tunes  $(Q^+ + Q^-) \pmod{1} < 1$ . The schematic resonance diagram for  $N = 1$  in Figure 3 shows the resonances in machines with errors for all  $N$ . Figures 1, 5–7, show examples of these resonances in the cases  $1 \oplus 1 = 1$ ,  $1 \oplus 1 = 2$ ,  $2 \oplus 2 = 4$ , and  $3 \oplus 3 = 3$ , respectively. The growth rates displayed correspond to  $e$ -folding times of a few turns, making it rather unlikely that the resonances can be cured by a feedback system at present or in the near future.

## APPENDIX A BEAM–BEAM FAMILIES

In a machine of type  $N \oplus N = N_{\text{IP}}$ ,  $N_{\text{IP}}$  is at most  $2N$ . When some of these IPs are inactivated by separators, for example, it might happen that the one-turn matrix  $M_1$  can be blockwise diagonalized by reordering the basis vectors. When this happens, we call this case reducible. If the one-turn matrix cannot be blockwise diagonalized by any permutation of basis vectors, we call this case irreducible. The reducible one-turn matrix can be reduced to  $N_{\text{F}}$ , the number of families, irreducible diagonal blocks. When  $N_{\text{F}} = 1$ , the case is irreducible.

Each block of bunches, corresponding to an irreducible diagonal block, is called a (beam–beam) family. Bunches belonging to different families do

not interact with each other even indirectly: if we kick a bunch, the bunches belonging to the same family of the kicked bunch are eventually affected by the kick but those belonging to other families are not affected. Conversely, bunches belonging to different families do not collide with each other in any active IP. In this appendix, we show how to calculate  $N_F$ . A family is composed of one or more  $e^+$  bunches and the same number of  $e^-$  bunches. We consider the  $e^+$  bunches only because  $e^-$  bunches can be treated in the same manner.

We label IPs and bunches in a different way from the main text. Each beam is composed of  $N$  equidistant bunches. The  $e^+$  beam rotates clockwise and the  $e^-$  counterclockwise in the ring. Possible IPs are labelled clockwise as  $IP_i$ ,  $0 \leq i \leq 2N - 1$ . Bunches are called clockwise  $e_j^\pm$ ,  $0 \leq j \leq N - 1$ . The chronological step is numbered as  $t_k$ ,  $k = \dots, -2, 0, 2, \dots$ . At  $t_0$ ,  $e_j^+$  and  $e_j^-$  sit at  $IP_{2j}$ . It is convenient to define these numbers in a cyclic manner:  $e_j^\pm$  is identical with  $e_{j+nN}^\pm$ ,  $IP_i$  with  $IP_{i+2nN}$  and  $t_k$  with  $t_{k+2nN}$ , where  $n$  is any integer. The  $e_j^\pm$  bunch comes to  $IP_i$  at  $t_k$  as

$$i(\text{IP}) = 2j(\text{bunch}) \pm k(\text{time}) \bmod 2N. \quad (51)$$

Two bunches  $e_i^\pm$  and  $e_j^\pm$  are in the same family when  $e_i^\pm$  can influence  $e_j^\pm$  through a beam-beam interaction. We write

$$e_i^\pm \sim e_j^\pm.$$

If only one IP,  $IP_0$ , is active, each  $e^+$  bunch forms a family so that  $N_F$  is  $N$ .

Let us first consider the case where two IPs ( $IP_0$ ,  $IP_s$ ) are active. We can assume that  $1 \leq s \leq N$  without loss of generality. From (51),  $e_0^-$  collides with  $e_0^+$  at  $IP_s$  at  $t_{-s}$  and with  $e_0^+$  at  $IP_0$  at  $t_0$ . Repetition of this process yields

$$e_{-s}^+ \sim e_0^+ \sim e_s^+.$$

By repeating the same argument, we finally arrive at

$$e_0^+ \sim e_{ns}^+,$$

for any value of the integer  $n$ . Thus, the collisions at  $IP_0$  and  $IP_s$  cause all  $e_j^+$  with  $j = 0, s, 2s, \dots$  to be in one family. It follows that the number of families is

$$N_F = \text{gcd}(N, s), \quad (52)$$

where  $\text{gcd}$  stands for the greatest common divisor. Each family contains  $N/N_F$  bunches in each beam. In particular,  $N_F = 1$  when  $s = 1$  or when  $N$  is a prime number and  $N_F = N$  when  $s = N$  (two diametrically opposite IPs). The family due to two diametrically opposite IPs (i.e.  $\text{IP}_0$  and  $\text{IP}_N$ ) is identical with the family due to  $\text{IP}_0$  (or  $\text{IP}_N$ ) alone.

A simple consequence is that the family due to IPs of  $(\text{IP}_0, \text{IP}_s, \text{IP}_N)$  is identical with the family due to  $(\text{IP}_0, \text{IP}_s)$ . The proof is as follows: Consider a family due to  $(\text{IP}_0, \text{IP}_s)$ . This family might interact with other families (so that families will merge) by introducing a new IP. By  $\text{IP}_N$ , however, this merging of families does not happen because  $\text{IP}_N$  defines the same family as  $\text{IP}_0$ . Hence, we need not consider the diametrically opposite IP. Another simple consequence is that the family due to  $(\text{IP}_0, \text{IP}_s, \text{IP}_{2s}, \dots, \text{IP}_K)$  is the same as the family due to  $(\text{IP}_0, \text{IP}_s)$ . The equidistant  $(K + 1)$  IPs define the same family so that the number of families  $N_F$  is also  $N_F = \text{gcd}(N, s)$ .

Let us now discuss machines with equidistant periodic IPs, in which  $N_{\text{IP}}$  must be a divisor of  $2N$ . We can apply the discussion above using  $s = 2N/N_{\text{IP}}$ . All possibilities for  $N_F = \text{gcd}(N, s)$  are listed in Table VIII.

For LEP with complete separation at the odd pits, the IPs are  $(\text{IP}_0, \text{IP}_2, \text{IP}_4, \text{IP}_6)$  and  $N = 4$ . Thus  $N_F = \text{gcd}(4, 2) = 2$ . For Furman's case<sup>16,17</sup>  $N = 26$  and active IPs are  $(\text{IP}_0, \text{IP}_4, \text{IP}_{26}, \text{IP}_{30})$ . The  $\text{IP}_0$  and  $\text{IP}_{26}$  are a diametrically opposite pair and so are  $\text{IP}_4$  and  $\text{IP}_{30}$ . Thus the family structure is the same as that due to  $(\text{IP}_0, \text{IP}_4)$ , and we have  $N_F = \text{gcd}(26, 4) = 2$ . More general and complicated cases can be discussed in the same manner.

The discussion given here applies to machines with errors as well as without errors because it depends only on the geometrical configuration of the collisions.

TABLE VIII Number of families  $N_F$  for perfectly periodic  $N \oplus N = N_{\text{IP}}$  cases, where  $m$  is a divisor of  $N$  (if any) but not 1, 2 or  $N$

$N_{\text{IP}}$	1	2	$m$	$m$	$N$	$N$	$2N$
$N_F$	$N$	$N$	$N/m$	$2N/m$	1	2	1
when	always	always	$N$ odd	$N$ even	$N$ odd	$N$ even	always





- [4] Piwinski, A. (1979). *IEEE Trans. Nucl. Sci.*, **NS-26**, 4268.
- [5] Satoh, K. (1987). *Proc. 6th Symp. Accel. Sci. Tech. (Tokyo)*, 18.
- [6] Talman, R. (1987). *AIP Conf. Proc.*, **153**, 789.
- [7] Ieiri, T., Kawamoto, T. and Hirata, K. (1988). *Nucl. Instrum. Methods*, **A265**, 364.
- [8] Arzelier, G., *et al.* (1971). *Proc. 8th Int. Conf. High-Energy Accel. (CERN)*, 150.
- [9] Derbenev, Ya.S. (1972). 3rd All-Union Conf. on Accel. (Moscow, 1972) 382, cf. SLAC TRANS 151.
- [10] Nguyen Ngoc Chau and Potaux, D., Laboratoire de l'Accélérateur Linéaire, Orsay, Rapport Technique 5-74 (1974) and 2-75 (1975).
- [11] Hirata, K. and Keil, E. (1989). *Phys. Lett.*, **B232**, 413.
- [12] Piwinski, A. (1971). *Proc. 8th Int. Conf. High-Energy Accel. (CERN)*, 357.
- [13] Chao, A. and Keil, E. (1979). CERN/ISR-TH/79-31.
- [14] Keil, E. (1980). LEP Note 226.
- [15] Keil, E. (1980). LEP Note 268.
- [16] Furman, M.A. and Chao, A.W. (1985). *IEEE Trans. Nucl. Sci.*, **NS-32**, 2297.
- [17] Furman, M.A. (1986). SSC-62.
- [18] Keil, E. (1981). *Nucl. Instrum. Methods*, **188**, 9.
- [19] Hofmann, A. and Myers, S. (1988). LEP Note 604.
- [20] Bambade, P. *et al.* (1988). *Phys. Rev. Lett.*, **62**, 2949.
- [21] Hirata, K. and Keil, E. (1989). CERN-LEP-TH/89-57.
- [22] Keil, E. (1992). CERN SL/92-29, 373.
- [23] Meller, R.E. and Siemann, R.H. (1981). *IEEE Trans. Nucl. Sci.*, **NS-28**, 2431.
- [24] Yokoya, K. and Koiso, H. (1989). *Part. Accel.*, **27**, 181.
- [25] Courant, E.D. and Snyder, H.S. (1958). *Ann. Phys. (N.Y.)*, **3**, 1.
- [26] Forest, E. (1987). *Part. Accel.*, **21**, 133.
- [27] Bassetti, M. (1989). *Proc. 11th Int. Conf. High-Energy Accel. (Geneva)*, 650.
- [28] Vignola, G., Talk at workshop on physics and detectors for DAΦNE (Frascati, Italy).
- [29] Hirata, K. and Keil, E. (1991). *IEEE Part. Accel. Conf. (San Francisco)*, 482.
- [30] Keil, E., Cornelis, K. and Hirata, K. (1992). *Proc. 15th Int. Conf. High-Energy Accel. (Hamburg 1992)* 1106; cf. CERN SL 92-33 (DI).